WHIOCE PUBLISHING PTE. LTD.
PROVIDING
FIRST-CLASS SCIENTIFIC INFORMATION
FOR TOP SCHOLARS

——ONLINE FIRST(NOT Peer-Reviewed)——

Title：Three-dimensional boundary layer flow of nanofluids due to an unsteady stretching surface

Author：A. Mahdy

Institute/Affiliation：South Valley University

Process：1、First trial(Field and check) ✓

2、Peer review ☐

3、Editing and three trials ☐

4、Published online ☐

Whioce Publishing Pte. Ltd. Singapore

Three-dimensional boundary layer flow of nanofluids due to an unsteady stretching surface

A. Mahdy

Mathematics Department, Faculty of Science, South Valley University, Qena, Egypt

mahdy@svu.edu.eg

Abstract

A numerical solution has been obtained for the unsteady three-dimensional stretching flow and heat transfer due to uncertainties of thermal conductivity and dynamic viscosity of nanofluids. The term of nanofluid refers to a solid–liquid mixture with a continuous phase which is a nanometer sized nanoparticle dispersed in conventional base fluids. The unsteadiness in the flow and temperature fields is caused by the time-dependent of the stretching velocity and the surface temperature. Different water-based nanofluids containing Cu, Ag, and TiO_2 are taken into consideration. The governing partial differential equations with the auxiliary conditions are converted to ordinary differential equations with the appropriate corresponding conditions via scaling transformations. Comparison with known results for steady state flow is presented and it found to be in excellent agreement.

Keywords: Nanofluid; unsteady state; three-dimensional; boundary layer.

Nomenclature

a	Constant
A	Unsteadiness parameter
B	Magnetic flux density
c_p	Specific heat at constant pressure
f	Dimensionless stream function
L	Slip length
Mn	Magnetic field parameter
Pr	Prandtl number
Q_0	Heat generation or absorption coefficient
S	Suction or injection parameter
t	Time
T	Temperature of the fluid
(u, v)	Velocity components of the fluid

U Velocity of stretching sheet

(x, y) Coordinate axes

Greek symbols

a Thermal diffusivity

l Dimensional heat generation/absorption parameter

s Electrical conductivity

r Density of the fluid

y Stream function

n Kinematic viscosity

g Constant

q Dimensionless temperature

h Similarity variable

Subscripts

w Conditions at the wall

$¥$ Conditions in the free stream

Introduction

Analysis of the problem

An unsteady three-dimensional boundary layer flow of a quiescent viscous and incompressible nanofluid caused by the stretching of an infinite surface in two lateral directions x and y which also varies with time namely ($u_w = Ax/t, v_w = By/t)$) is considered. It is at rest at infinity and satisfies the no slip condition at the stretching surface and it has no lateral directions at z . The fluid is a water based nanofluid containing different types of nanoparticles such as Copper Cu, Titanate TiO_2, Silver Ag and Alumina Al_2O_3. It is assumed that the base fluid and the nanoparticles are in thermal equilibrium and no slip occurs between them. The thermo physical properties of the nanofluid are given in Table 1. The viscous dissipation terms are neglected. The boundary layer and Boussinesq approximations are assumed to be valid. The basic unsteady conservation of mass, momentum and thermal energy equations for nanofluids can be written in the form

$$\frac{\partial u}{\partial x} + \frac{v}{y} + \frac{\partial w}{\partial z} = 0 \tag{1}$$

$$r_{rf}\left[\frac{\partial u}{\partial t} + u\frac{u}{x} + v\frac{\partial u}{\partial y} + w\frac{u}{z}\right] = m_{rf}\frac{\partial^2 u}{\partial z^2} \tag{2}$$

$$r_{rf}\left[\frac{\partial v}{\partial t} + u\frac{v}{x} + v\frac{\partial v}{\partial y} + w\frac{v}{z}\right] = m_{rf}\frac{\partial^2 v}{\P z^2} \qquad (3)$$

$$(r c_p)_{rf}\left[\frac{\partial T}{\partial t} + u\frac{T}{x} + v\frac{\partial T}{\partial y} + w\frac{T}{z}\right] = k_{rf}\frac{\partial^2 T}{\P z^2} \qquad (4)$$

In the above equations x, y are rectangular coordinates parallel to the surface; z is the coordinate perpendicular to the surface; u, v, w are the velocity components in x, y, z

directions, respectively, t is the time, r_{rf} is the effective density of the nanofluid, m_{rf} is the

effective dynamic viscosity of the nanofluid, T is the temperature of the nanofluid inside the thermal boundary layer, g is the acceleration due to gravity. Now for nanofluids let us introducing the expressions for m_{rf}, r_{rf} and $(r c_p)_{rf}$ as

$$m_{rf} = m_f(1 - f)^{-2.5}, \qquad r_{rf} = (1 - f)r_f + f r_s, \qquad (r c_p)_{rf} = (1 - f)(r c_p)_f + f(r c_p)_s \quad (5)$$

On the other hand, effective thermal conductivity can be calculated from the well-known formula Hamilton and Crosser (1962) and others as

$$\frac{k_{rf}}{k_f} = \frac{(k_s + 2k_f) - 2f(k_f - k_s)}{(k_s + 2k_f) + f(k_f - k_s)}$$

Furthermore, f is the solid volume fraction, m_f is the dynamic viscosity of the base fluid,

r_f, r_s are the densities of the base fluid and nanoparticle, respectively, k_f is the thermal

conductivity and $(r c_p)_{rf}$ is the heat capacity of the nanofluid, k_f, k_s are the thermal

conductivities of the base fluid and nanoparticle, respectively. The properties of the nanofluids shown in the above subjects are calculated from water and nanoparticle properties at bulk temperature. Following the method of group transformations (Ma and Hui [10]), we derive the group-invariant solutions of unsteady three-dimensional flow due to a stretching flat surface placed in a gradient fluid, where the stretching velocities of the surface along x and y directions and the similarity variables are described as

$$h = \frac{z}{\sqrt{n_f t}}, \quad u = \left(\frac{A x}{t}\right)f', \quad v = \left(\frac{A y}{t}\right)s', \quad w = -A\sqrt{n_f / t}(f + s), \quad q = \frac{T - T_\infty}{T_w - T_\infty} \qquad (6a)$$

$$u_w = \frac{A x}{t} \quad (A > 0, t > 0), \qquad v_w = \frac{B x}{t} \quad (B > 0, t > 0) \qquad (6b)$$

The relevant boundary conditions of the governing equations are

$$z = 0: \quad u = u_w, \quad v = v_w, \quad w = 0, \quad T = T_w \tag{7a}$$

$$z \to \infty: \quad u \to 0, \quad v \to 0, \quad T \to T_\infty \tag{7b}$$

With the change of variables (6), Eq. (1) is identically satisfied and Eqs. (2)–(4) are transformed to

$$\frac{1}{(1-f)^{2.5}\left[1-f+f\left(\frac{\rho_s}{\rho_f}\right)\right]}f''' + A(f+s)f'' - Af'^2 + \left(f'' + 2^{-1}hf''\right) = 0 \tag{8}$$

$$\frac{1}{(1-f)^{2.5}\left[1-f+f\left(\frac{\rho_s}{\rho_f}\right)\right]}s''' + A(f+s)s'' - As'^2 + \left(s'' + 2^{-1}hs''\right) = 0 \tag{9}$$

$$\frac{(k_{rf}/k_f)}{Pr\left[1-f+f\left(\frac{\rho c_p)_s}{\rho c_p)_f}\right)\right]}q'' + A(f+s)q' + 2^{-1}hq' = 0$$

$$\tag{10}$$

The transformed boundary conditions are turn into

$$h = 0: \quad f = 0, \quad f'' = 1, \quad s = 0, \quad s' = g, \quad q = 1$$

$$h \to \infty: \quad f'' \to 0, \quad s' \to 0, \quad q \to 0 \tag{11}$$

Here prime denotes ordinary differentiation with respect to the similarity independent variable h. In addition, $Pr = \nu_f/\alpha_f$ is the Prandtl number, $A, B, g\,(= B/A)$ are dimensionless constants and $g\,(0 \leq g \leq 1)$ is zero for a two-dimensional case and 1 for axisymmetric case. The steady-state equations are obtained by omitting the last term (given within the bracket) in Eqs. (8)-(10) which represents the unsteady effect.

Numerical procedure

An efficient Runge–Kutta fourth order method along with shooting technique was used to solve coupled ordinary differential equations Eqs. (8)-(10) with boundary conditions (11) for different values of controlling parameters. The asymptotic boundary conditions given by Eq. (11) were replaced by using a value of 4 for the similarity variable h as follows.

$$h_{max} = 4, \quad f'' \to 0, \quad s' \to 0, \quad q \to 0$$

The choice of $h_{max} = 4$ ensured that all numerical solutions approached the asymptotic values correctly. In the absence of nanoparticles ($f = 0$), the dimensionless heat transfer rates $q'(0)$ are compared with the literature [33, 35] in Table 1 and 2. Both results are found to be in good agreement. Therefore, we believe that the present results are accurate.

Results and discussion

The variation of velocity components in x and y directions (i.e. f' and s') for various values of g is plotted in Fig. 1 considering Cu-water nanoparticle and pure water. As it observed an increase in g tends to decrease the x velocity component f' whereas increase the y velocity component s'. Fig. 2 illustrate the effect of the constant A on both of f' and s', with increasing A both of f' and s' decrease.

Fig. 3 exhibits the velocity components distributions for different nanoparticles, when $A = 0.5$ $g = 0.6$ and $Pr = 6.2$ .It can be observed that the velocity temperature distributions for different nanoparticles and decrease gradually far away from the surface of the stretching sheet. Moreover, a slight increasing in the velocity and temperature distributions can be detected by adding different nanoparticles base fluid. Therefore, both Fig. 4 exhibits that the addition of to the different types of nanoparticles in water improves velocity profiles and temperature distributions. Moreover, it can be observed that the velocity profiles and the temperature distributions are not strongly affected by additional various nanoparticles with low solid volume fraction concentrations. In addition, it can be noticed in Fig. 4 that the velocity profiles of –water nanofluid are the higher one and normally Al greater the pure water. This figure show that on using different kinds of nanofluids the velocity and temperature change, which means that the nanofluids will be important in the cooling heating processes the

than
The obtained similarity system (6) - (8) is non-linear, coupled, ordinary differential equations, which possess no closed-form solution. Therefore, the system of equations (6)–(7), along with the boundary conditions (8) are solved numerically by means the very robust symbolic computer algebra software MATLAB employing the routine bvpc45. In addition, to validate the method used in this study and to judge the accuracy of the present analysis, comparison with available results of Chamkha et al. [26] and Sharidan et al. [25] corresponding to the skin-friction coefficient f_w ii

for unsteady flow of viscous incompressible fluid is made (Table 1) and found in excellent agreement. In order to get a clear insight of the behavior of velocity and temperature fields for non-Newtonian Casson fluid, a comprehensive numerical computation is carried out for various values of the parameters that describe the flow characteristics, and the results are reported graphically.

Figs. 1 and 2 illustrate the behavior of x -component of the translational velocity and temperature distributions, respectively, for different values of slip parameter. The slip parameter d measures the amount of slip at the surface. It is observed that, the velocity distribution decreases with the increasing values of slip parameter. Consequently, with the increase of slip parameter the thickness of boundary layer increases. It can further be noted that as d , the velocity of the fluid at the surface will coincide with the free stream velocity of the fluid, because if we increase the slip parameter d to a value tending to infinity then the boundary layer structure will disappear. Moreover, the temperature distribution increases with increasing the slip parameter. Figs. 3 and 4, respectively, depict the effects of the magnetic field parameter Mn on the fluid velocity and temperature distributions, considering the cases of wall mass suction and wall mass injection. Application of a magnetic field normal to an electrically-conducting fluid has the tendency to produce a drag-like force called the Lorentz force which acts in the direction opposite to that of the flow, causing a flow retardation effect. This causes the fluid velocity to decrease. However, this decrease in flow speed is accompanied by corresponding increases in the fluid thermal state level. These behaviors are clearly depicted in the decrease in the fluid velocity and the increase in the fluid temperature in figures 3-4. Furthermore, the magnetic parameter tends to decrease velocity gradient at the wall and increase temperature gradient as seen in Figs. 17 and 18. The velocity gradient as well as temperature gradient tends to decreases or increases rapidly at first, then gradually levels off as the non-Newtonian Casson parameter is increased. It is clear from these figures that both of f_w^{ii} and $-q_w'$ decrease with increasing values of the magnetic field parameter.

Influences of Casson parameter b on velocity and temperature distributions for unsteady motion are clearly depicted in Figs. 5 and 6, respectively considering wall mass suction and wall mass injection effects (i.e. $S = 0.4, -0.4$). The same type of behavior of velocity with increasing b is noted. The effect of increasing values of b is to reduce the velocity, and hence, the boundary layer thickness decreases. The increasing values of the Casson parameter i.e. the decreasing yield stress (the fluid behaves as Newtonian fluid as Casson parameter becomes large) suppress the velocity field. It is observed that $f'(h)$ and the associated boundary layer thickness are decreasing function of b . The velocity curves in Fig. 5 show that the rate of transport is considerably reduced with the increase of b . The effect of increasing b leads to enhance the temperature field for unsteady motion (Fig. 6). This effect is more pronounced for steady motion. The thickening of the thermal boundary layer occurs due to increase in the elasticity stress parameter. It can also be seen from Fig. 5 that the momentum boundary layer thickness decreases as b increases and hence induces an increase in the absolute value of the velocity gradient at the surface. Figs. 7 and 8 exhibit the velocity and temperature distributions, respectively for several values of unsteadiness parameter A . It is observed that the velocity along the sheet decreases initially with the increase in unsteadiness parameter A , and this implies an accompanying reduction of the thickness of the momentum boundary layer near the wall. The steady case is obtained when $A = 0$. Furthermore, it is noticed that the temperature at a particular point is found to decrease significantly with increasing unsteadiness parameter. The

effect of effect of heat generation or absorption parameter l on the temperature distributions is shown in Fig. 9. It is clear that as the heat generation or absorption parameter increases the temperature of the fluid increases as well as the temperature gradient increases (Fig. 20). Fig. 10 shows the behavior of the temperature distributions for the variation of Prandtl number, Prandtl number signifies the ratio of momentum diffusivity to thermal diffusivity. It is seen that the temperature decreases with increasing Pr. Moreover, the thermal boundary layer thickness decreases by increasing Prandtl numbers. Wall temperature gradient is negative for all values of Prandtl number as seen from Fig. 19 which means that the heat is always transferred from the surface to the ambient fluid. An increase in Prandtl number reduces the thermal boundary layer thickness. Fluids with lower Prandtl number will possess higher thermal conductivities (and thicker thermal boundary layer structures), so that heat can diffuse from the sheet faster than for higher Pr fluids (thinner boundary layers). Figs. 11 and 12 display the effects of suction/blowing parameter s on velocity and temperature fields. With increasing s, fluid velocity is found to decrease. That is, the effect of s is to decrease the fluid velocity in the boundary-layer and in turn, the wall shear stress decreases. The increase in s causes thinning of the boundary layer. However, temperature at a point is found to decrease with increasing s. This causes a decrease in the rate of heat transfer.

The behavior of rate of heat transfer (from the sheet to the fluid) decreases with increasing A as observed from Fig. 13. As the unsteadiness parameter A increases, less heat is transferred from the sheet to the fluid; hence, the temperature $q(h)$ decreases (Fig. 8). Since the fluid flow is caused solely by the stretching sheet, and the sheet surface temperature is higher than free stream temperature, the velocity and temperature distributions decrease with increasing h. It is important to note that the rate of cooling is much faster for higher values of unsteadiness parameter, whereas it may take longer time for cooling during steady flows. Moreover, Fig. 14 displays the influences of unsteadiness parameter A and Casson parameter b on velocity gradient at the wall $f_w{}^{ii}$. Magnitude of $f_w{}^{ii}$ related to skin-friction coefficient decreases with increasing unsteadiness parameter A and also with Casson parameter b, but the magnitude of temperature gradient at the surface decreases for b and A. A drop in skin-friction as investigated in this paper has an important implication that in free coating operations and elastic properties of the coating formulations may be beneficial for the whole process. This means that less force may be needed to pull a moving sheet at a given withdrawal velocity, or equivalently higher withdrawal speeds can be achieved for a given driving force resulting in, increase in the rate of production. Figs. 15 and 16 illustrate the effect of slip parameter on velocity and temperature gradient, respectively. As it is illustrated, both of velocity and temperature gradient increase with the increase of slip flow parameter.

Conclusions

In this paper, the mechanical and thermal properties of unsteady MHD boundary layer slip flow of a non-Newtonian Casson fluid past a vertical stretching surface taking into account the wall mass suction or injection and heat generation or absorption effects have been investigated systemically. With the help of appropriate similarity transformation, the governing time

dependent boundary layer equations for momentum and thermal energy are reduced to coupled non-linear ordinary differential equations which are then solved numerically. Results for the velocity and temperature distributions as well as velocity gradient f_w^{ii}, temperature gradient $q_w^{¢}$ are presented for representative governing parameters. As a summary, we can conclude that

- Fluid velocity decreases initially due to increase in unsteadiness parameter; temperature also decreases significantly in this case.
- The effect of increasing values of the Casson parameter is to suppress the velocity field, whereas the temperature is enhanced with increasing Casson parameter. Moreover, Slip parameter and magnetic field parameter have the same effects.
- Both of f_w^{ii} and $q_w^{¢}$ increase with the increase of slip flow parameter, whereas the magnetic field and unsteadiness parameters have an opposite effect. In addition, f_w^{ii} decreases while $q_w^{¢}$ increases with increasing Casson parameter.
- Prandtl number can be used to increase the rate of cooling in conducting flows.
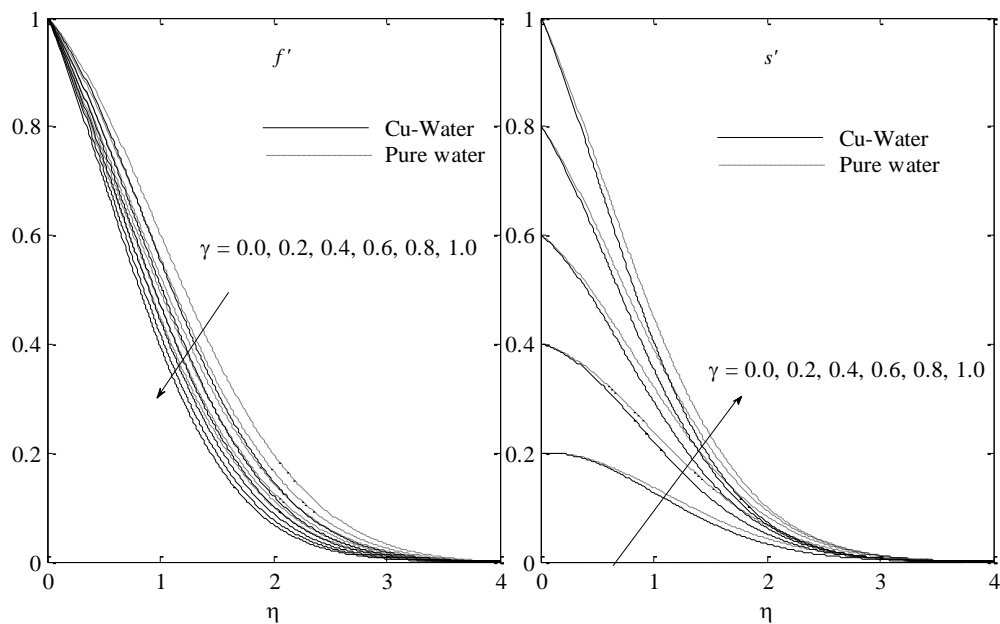
Fig. 1 Velocity components f' and s' distributions for different values of g
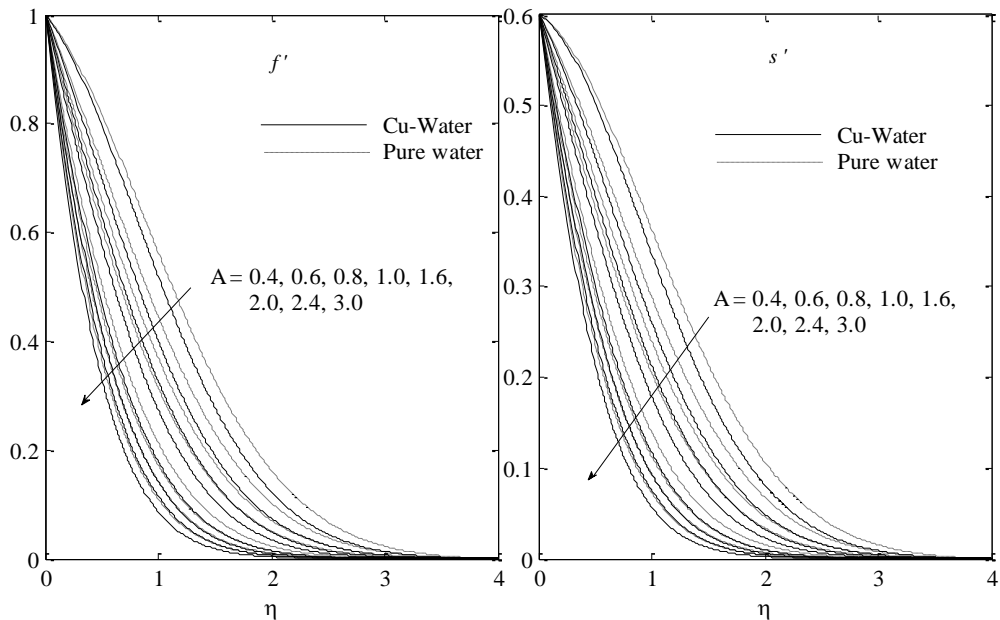
Fig. 2 Velocity components f' and s' distributions for different values of A
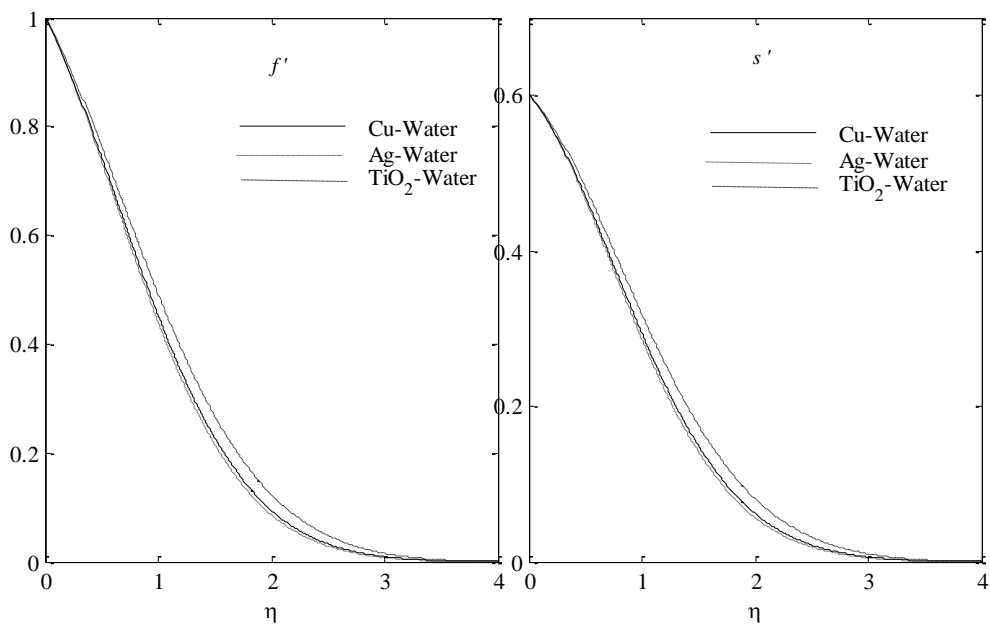
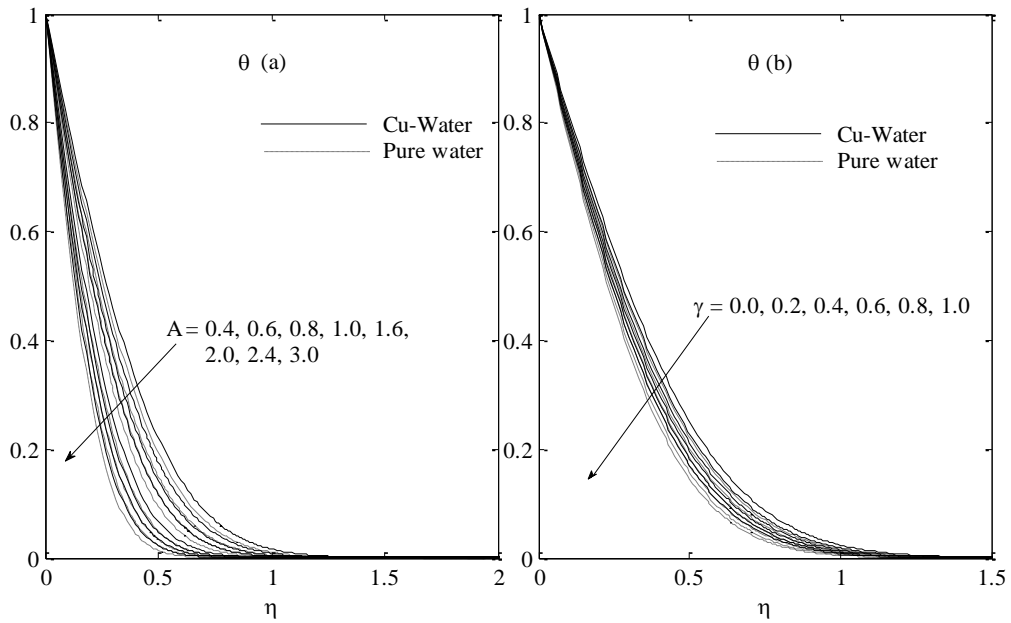Fig. 3 Velocity components f' and s' distributions for different nanoparticles

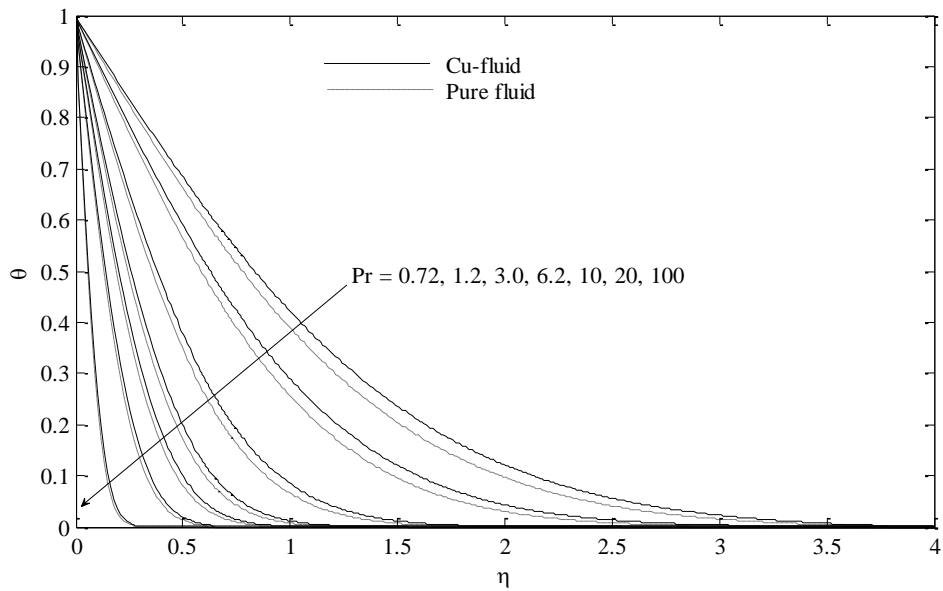Fig. 4 Temperature θ distribution for different values of (a)A, (b)γ

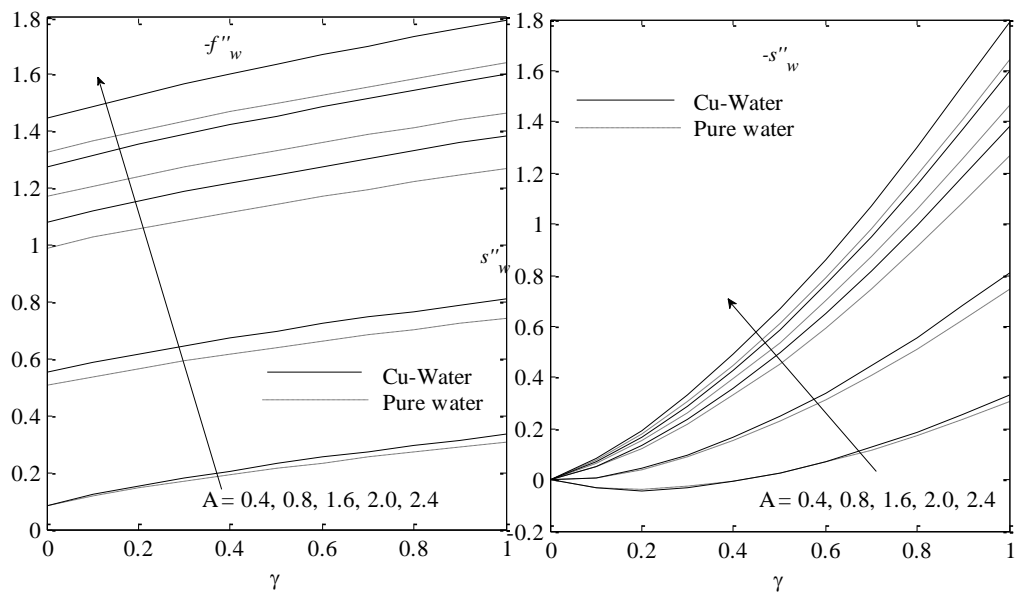Fig. 5 Temperature θ distribution for different values of Pr

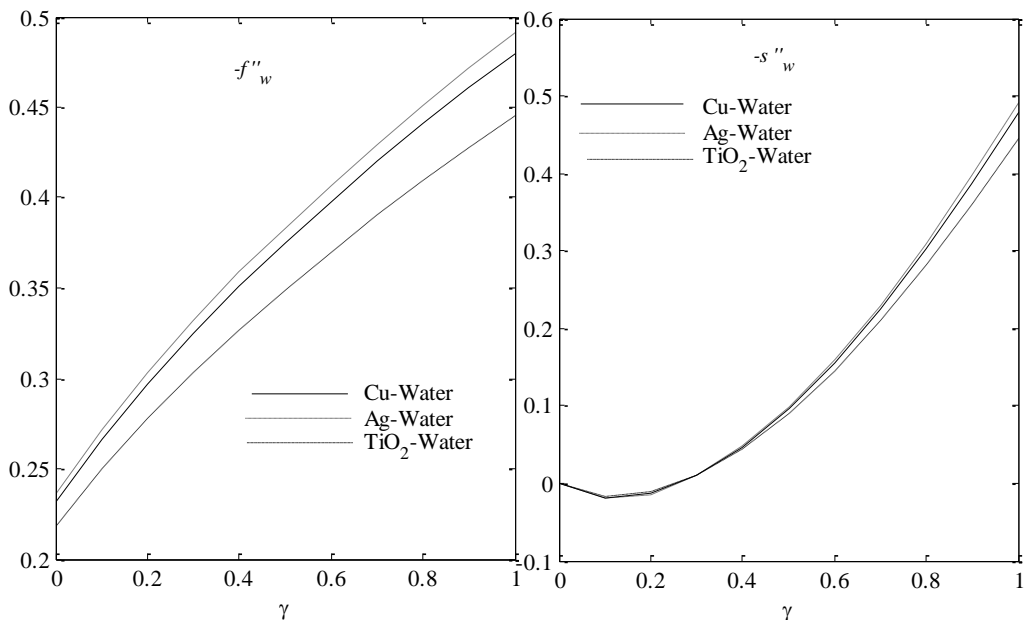Fig. 6 Variations of $-f_w''$ and $-s_w''$ against g for different values of A

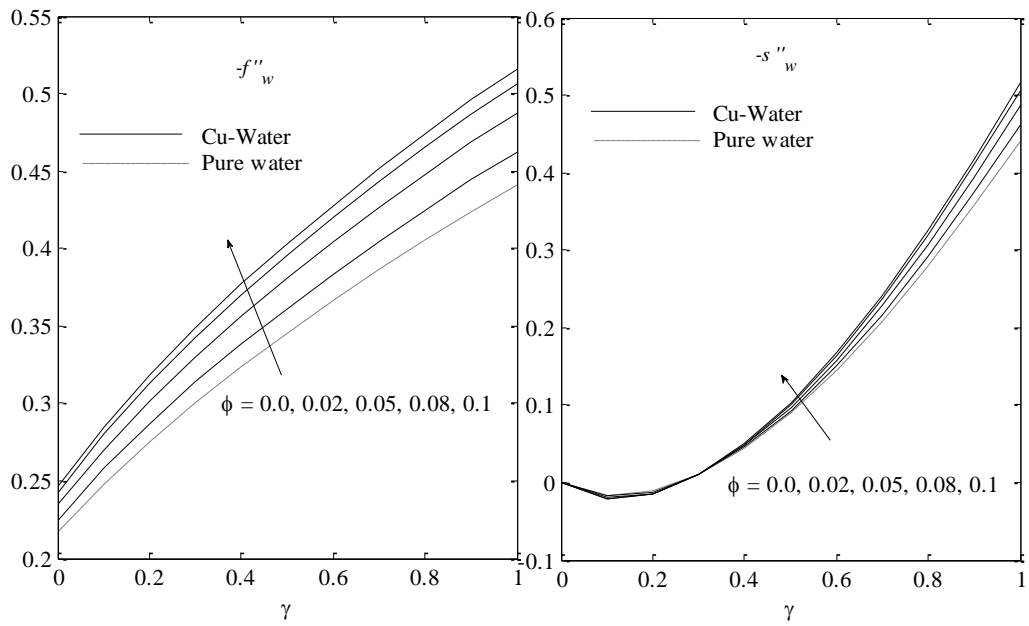Fig. 7 Variations of $-f_w''$ and $-s_w''$ against g for different nanoparticles

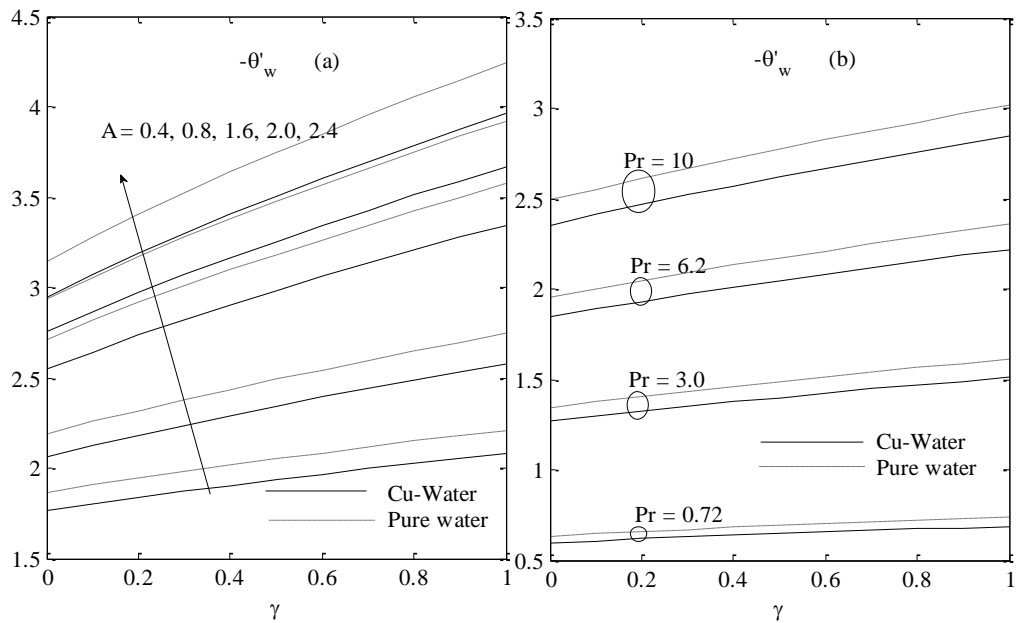Fig. 8 Variations of $-f''_w$ and $-s''_w$ against g for different nanoparticle solid volume fraction f

Fig. 9 Variations of $-q'_w$ against g for different values of (a) A, (b) Pr

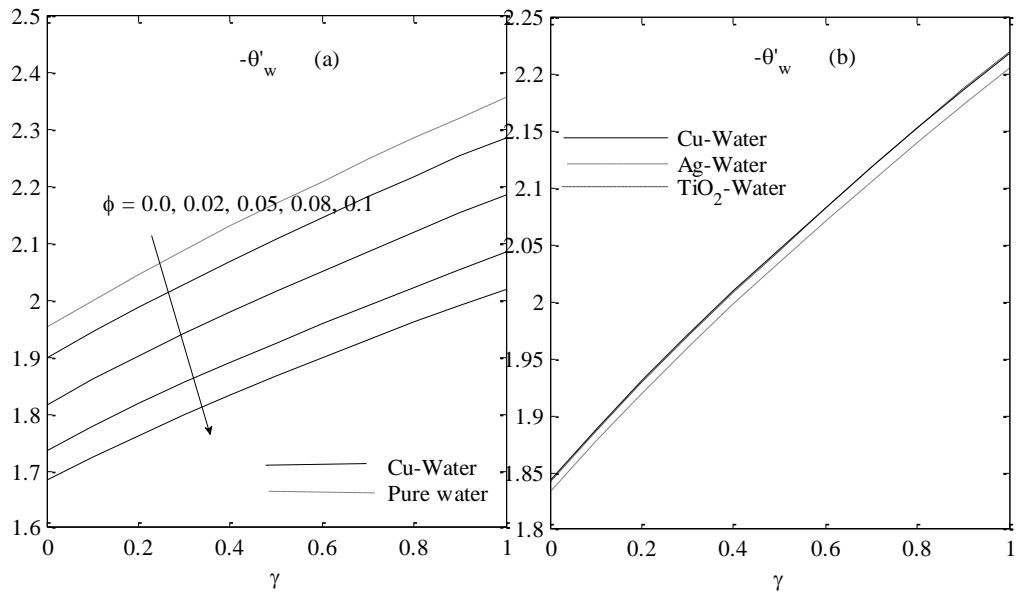Fig. 10 Variations of $-q_w'$ against g for different values of (a) f, (b) nanoparticles